Rapid Healing

How hydrogenation supercharges recovery of electron-irradiation defects in Ga-doped PERC solar cells

Li, Guo; Zhou, Zhuangyi; Madumelu, Chukwuka; Toth, Peter; van den Hengel, Lennart; Grozema, Ferdinand; Conibeer, Gavin; Hoex, Bram

DOI
10.1016/j.solmat.2025.113729

Publication date
2025

Document Version
Final published version

Published in
Solar Energy Materials and Solar Cells

Citation (APA)
Li, G., Zhou, Z., Madumelu, C., Toth, P., van den Hengel, L., Grozema, F., Conibeer, G., & Hoex, B. (2025). Rapid Healing: How hydrogenation supercharges recovery of electron-irradiation defects in Ga-doped PERC solar cells. *Solar Energy Materials and Solar Cells*, *290*, Article 113729. https://doi.org/10.1016/j.solmat.2025.113729

Solar Energy Materials & Solar Cells 290 (2025) 113729

Contents lists available at ScienceDirect

Solar Energy Materials and Solar Cells

journal homepage: www.elsevier.com/locate/solmat

Rapid Healing: How hydrogenation supercharges recovery of electron-irradiation defects in Ga-doped PERC solar cells

Guo Li [a], Zhuangyi Zhou [a], Chukwuka Madumelu [a], Peter Toth [b], Lennart van den Hengel [c], Ferdinand Grozema [c], Gavin Conibeer [a], Bram Hoex [a,*]

[a] School of Photovoltaic and Renewable Energy Engineering, University of New South Wales, Sydney, NSW, 2052, Australia
[b] Extraterrestrial Power Pty Ltd, Cronulla, 2230, NSW, Australia
[c] Faculty of Applied Sciences, Delft University of Technology, 2629, HZ Delft, the Netherlands

A B S T R A C T

Due to significantly lower costs than compound semiconductor counterparts, there is increasing interest in using silicon solar cells for cost-sensitive space missions, particularly in low Earth orbit (LEO). A major concern is, however, that the minority carrier lifetime (lifetime) of silicon solar cells degrades severely under high-energy electron irradiation. Fortunately, thermal and hydrogenation processes can potentially recover all the irradiation losses. This work studies these defects and their recovery using contactless lifetime measurement and deep-level transient spectroscopy (DLTS). Both fired and unfired Ga-doped passivated emitter and rear contact (PERC) solar cell precursors are used in this work. The precursors were irradiated with 1 MeV electrons and annealed at 300 °C and 380 °C, respectively. All the samples exhibited lifetime recovery, with fired samples recovering faster and achieving higher saturated lifetime. After ~360s of annealing at 380 °C, the irradiated fired samples recovered to their pre-irradiation lifetime, whereas the irradiated non-fired samples required 71.5 times longer (25,740 s). Remarkably, longer annealing caused reductions in lifetime, likely due to surface-related degradation. The DLTS measurements revealed a clear reduction of recombination-active defects after annealing, including V-V^+ and C_i-C_s in irradiated fired samples and V-V^+ in irradiated unfired samples. This study demonstrates that the firing process is critical for optimizing the recovery of irradiation damage in silicon solar cells. Hydrogenation of the silicon bulk results in quicker recovery and superior End-of-life performance compared to thermal recovery without hydrogen. Therefore, Ga PERC with bulk hydrogenation can recover radiation-induced damage, rendering it suitable for LEO missions.

1. Introduction

From the beginning of the space race until the 1990s, silicon solar cells were the dominant power source for space applications [1]. However, silicon electronic quality significantly degrades during space missions due to its weak irradiation tolerance. Performance loss occurs when high-energy space particles collide with silicon atoms in the lattice, creating recombination-active Shockley-Read-Hall traps [2]. These traps suppress the effective minority carrier lifetime (referred to henceforth as lifetime), resulting in a low End-of-Life (EoL) performance of irradiated silicon solar cell devices. In contrast, solar cells made from III-V semiconductors, like gallium arsenide (GaAs), have taken over the current space market, benefiting from superior irradiation tolerance, a higher Beginning-of-Life (BoL) efficiency, and lower weight. After exposure to 10^{15}/cm^{3}of 1 MeV electron irradiation, III-V solar cells can retain ~80–90 % of their performance [3–5]. III-V solar cells like $GaAs_{1-X}Sb_X$ show high irradiation tolerance with almost no V_{OC} degradation and over 80 % J_{SC} retention after 10^{15}/cm^3 of 1 MeV electron irradiation [4] and the multijunction III-V solar cells with a $Ga_{0.51}In_{0.49}P$/GaAs/$Ga_{0.73}In_{0.27}As$ subcell can retain 83 % of BoL performance after the same irradiation doses [5]. In contrast, silicon solar cells typically exhibit a Remaining Factor (RF) ranging from 50 % to 80 %, depending on their design [6,7], after the same electron dose.

Although silicon shows weaker irradiation tolerance, it is now opportune to reconsider using silicon solar cells for space applications for several reasons. Firstly, the performance of silicon solar cells has been significantly enhanced, from 15 % to over 26 % under the AM1.5G spectrum [8]. Meanwhile, the manufacturing cost of III-V solar cells is two or three magnitudes higher than commercial silicon solar cells [9], which means the current industrial silicon-based cells can potentially lower the cost of space missions, in particular for relatively short Low Earth Orbit (LEO) missions that demand lower irradiation stability than deep-space exploration. Thus, reintroducing silicon solar cells with enhanced lifetime recovery capabilities may be a cost-effective option for short-term LEO space missions.

To understand the complexity of irradiation damage, researchers

* Corresponding author.
E-mail address: b.hoex@unsw.edu.au (B. Hoex).

https://doi.org/10.1016/j.solmat.2025.113729
Received 14 February 2025; Received in revised form 11 May 2025; Accepted 16 May 2025
Available online 20 May 2025

have investigated the formation of irradiation-induced defects in silicon material for over five decades [10,11]. It has been found that the irradiation-induced defects are more complicated than the defects typically found in terrestrial silicon solar cells. For the standard silicon solar cell process, one of the impurities, phosphorus, boron, or gallium, is introduced as an electrically active dopant to manipulate the bulk carrier concentration [12]. Additional unfavorable contaminants, such as carbon and oxygen, are introduced during crystalline silicon's growth and can form complexes acting as recombination-active centers within the silicon bandgap [13]. In addition to these common defects/impurities, the collision between electrons/protons and silicon atoms introduces interstitial silicon atoms and vacancies within the lattice [14]. These vacancies are mobile and can later form di-vacancies [15] or react with carbon or oxygen in the silicon material to form recombination active complexes such as the A-center (oxygen-vacancy) [16] in both n-type and B-doped p-type silicon material. Generally, the p-type base silicon solar cells have better irradiation tolerance compared to the n-type base, and gallium-doped cells were found to be more irradiation stable than the boron-doped [17,18]. Remarkably, these defects can be removed with thermal processes [19,20]. In previous work, the annealing recovery of irradiation-induced defects from either electron [19,21–23], proton [23,24] or gamma radiation [20], was well explained using the deep-level transient spectroscopy (DLTS) technique. By applying pulsed bias voltage on silicon wafer with Schottky contact, the DLTS method can measure the transient electrical capacitances, hence identifying the deep-level defects. According to Khan et al. [19], the di-vacancies introduced by electron irradiation can be annealed out at 400 ° C for 10 min, and a similar recovery was also observed at lower temperatures (270–325 ° C) but with a longer annealing duration (15 min) [21]. Similarly, it was also shown that proton-induced damage could be recovered by annealing [24]. These results show that the annealing recovery of irradiation damage is temperature dependent, as such recovery is attributed to the interaction of vacancies and self-interstitials. However, such a self-healing process is extremely slow at relatively low operating temperatures, typically <100 ° C, during space missions. Thus, the temperature-independent recovery mechanism needs to be investigated to accelerate the recovery ability of space silicon solar cells. Recently, Khan et al. [25] observed that the fabrication of silicon devices can also bring a significant difference in the kinetics of irradiation defect recovery. The fired silicon samples exposed to 1 MeV electron irradiation showed significant performance recovery with subsequent thermal annealing at 150 ° C. However, it was observed that the non-fired samples did not recover using identical annealing conditions. Gaining insights into this mechanism may enhance engineering methods to increase the recovery ability of space silicon solar cells.

In this work, we will compare the recovery dynamics between fired and unfired samples. We will evaluate the irradiation damage and subsequent thermal recovery mechanism by using both Injection Dependent Lifetime Spectroscopy (IDLS) [26] and DLTS. Our study conducted at 300 °C and 380 °C shows that the fired samples recover significantly faster than their non-fired counterparts. This indisputably confirms that bulk hydrogenation is considerably more efficient in recovering radiation damage compared to thermal annealing. Consequently, our work provides a pathway to self-healing silicon solar cells that can be produced at a cost similar to terrestrial silicon solar cells, thus enabling significantly lower-cost LEO space missions.

2. Experimental details and methodologies

As the p-type silicon solar cells show a higher irradiation tolerance [17,18] and Ga-doped PERC solar cells are widely used in the current photovoltaic (PV) market, Ga-doped PERC precursors were used for this study. 15.8 cm × 15.8 cm Ga-doped PERC precursors were taken from an industrial manufacturing line before metallization and firing. As shown in Fig. 1, one group of Ga PERC precursors was bulk hydrogenated with a firing process with a peak temperature of 750 ° C using a Schmid 2500 Series Controlled Atmosphere Conveyor Furnace. Whereas for the unfired PERC precursors, no hydrogen was diffused into the bulk from the SiN_X layer and consequently hydrogen is only available to passivate defects at the c-Si interface.

Then, these samples were cut into 4 cm × 4 cm tokens and irradiated from the front side with a 5×10^{14} e/cm^2 total dose of 1 MeV electrons at the Delft University of Technology. The irradiation time was chosen based on the dose rate and target dose (5×10^{14} e/cm^2). The temperature of the irradiation table did not exceed 23 ° C during the irradiation process. Some unfired and fired samples were not irradiated and kept as a control.

Following the electron irradiation, the samples were dark annealed using an IKAC-MAG HP 10 hotplate. Based on previous work [19,24], the hotplate temperature was set at 300 ° C and 380 ° C, respectively. These elevated temperatures were chosen to accelerate defect recovery and enable a more efficient assessment of irradiation-induced defect passivation. Future work will investigate recovery behavior at lower, more moderate temperatures under illumination, as this condition is more relevant to space environments. To evaluate the effects of electron irradiation and dark annealing process on the lifetime, a Sinton WCT-120 tool was employed, enabling contactless *ex-situ* IDLS measurements. The effective lifetime was measured before irradiation, after irradiation and intermittently during the dark annealing recovery. The effective lifetime has reciprocal relations among the lifetime components, including intrinsic recombination lifetime τ_i, SRH lifetime τ_{SRH} and surface lifetime τ_s. Where the τ_i includes radiative τ_{rad} and Auger lifetime τ_{Aug}. And the τ_s is directly corresponded with the surface recombination current, J_0. Thus, the effective lifetime can be written as follows:

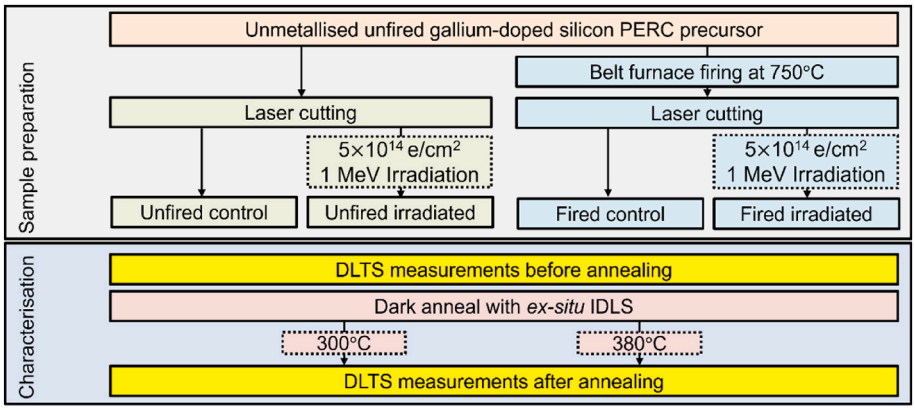

Fig. 1. The experimental workflow used in this work.

$$\tau_{eff}^{-1} \cong \tau_{rad}^{-1} + \tau_{Aug}^{-1} + \tau_{SRH}^{-1} + \frac{J_{0,front}(N_A + \Delta n)}{dqn_i^2} + \frac{J_{0,rear}(N_A + \Delta n)}{dqn_i^2} \quad (1)$$

Where N_a is the acceptor density, d the sample thickness, q the elementary charge, $J_{o,front}$ and $J_{0,rear}$ the front and rear surface saturation current density, respectively, and n_i the intrinsic carrier density. Both τ_{rad} and τ_{Aug} are intrinsic properties of silicon material and the irradiation damage variation in τ_{eff} manifests itself through the variation of τ_{SRH} and J_0. To evaluate the level of degradation and recovery, the normalized defect density (NDD) value is used in this work to quantify the defect density [27]. It can be written as:

$$NDD = \tau_{eff}^{-1}(t) - \tau_{eff.BoL}^{-1} \quad (2)$$

Where the $\tau_{eff}(t)$ is the effective lifetime of PERC precursors after incremental steps of the dark annealing process, and the $\tau_{eff.BoL}$ is the effective lifetime of the same sample prior to the irradiation process. The effective lifetime values are extracted at the same injection level (MCD $= 10^{15}/cm^3$). As the resistivity of our tested sample changed under 380 ° C dark annealing, the lifetime and NDD were calculated based on the actual resistivity.

DLTS measurements were carried out to investigate the electrically active defects using a PhysTech FT-1030 HERA DLTS tool. As the DLTS measurements on Schottky barrier diodes (SBDs) only probe the space charge region near the contact, a significant amount of surface material (~5 μm) was removed before the metal contacts were evaporated, allowing us to obtain the bulk relevant signals after irradiation. The silicon samples were measured: before annealing, fully recovered, and after extended annealing. DLTS measurements were conducted using the samples cleaved from the same lifetime tokens to minimize the difference from sample to sample. The following steps are applied to prepare the DLTS samples:

(1) Mechanical polishing using a Tegramin-25 tool from Struers to remove the samples on the diffused side for ~5 μm (including SiN_X and the diffused layer) until the surface was mirror polished,
(2) Radio Corporation of America (RCA) cleaning,
(3) Rear side SiN_X layer removal using 4.9 % HF solution until hydrophobic,
(4) DI-Wafer rinse for 5 min to remove any residual HF,
(5) Aluminum and gold evaporation using a Lesker physical vapor deposition (PVD) 75 electron beam evaporation tool to form front Schottky and rear Ohmic contact, respectively.

3. Results and discussion

3.1. Stability of the unirradiated control samples

To demonstrate the thermal stability of the Ga PERC samples used in

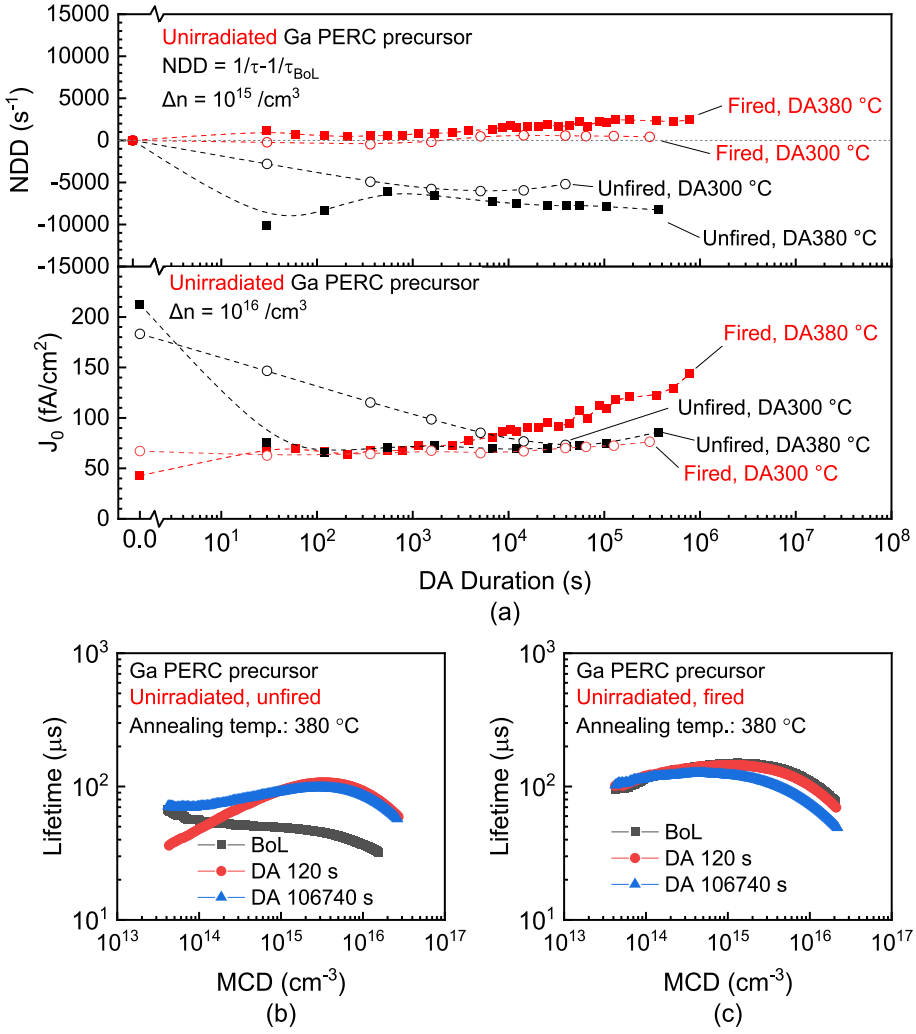

Fig. 2. (a) NDD and J_0 results of unirradiated unfired (black) and fired (red) PERC as a function of the dark annealing time. The NDD was calculated at an injection level of $10^{15}/cm^3$. (b) Unfired/(c) fired, injection dependent effective lifetime of unirradiated PERC after 0 s (BoL, black), 120 s (red) and 106,740 s (blue) of 380 ° C dark annealing. (For interpretation of the references to color in this figure legend, the reader is referred to the Web version of this article.)

this study, the NDD value of the control samples is presented as shown in Fig. 2 (a). These unirradiated control samples were annealed at the same condition as the irradiated samples, *i.e.*, 300 and 380 ° C. The IDLS curves for unfired and fired samples are shown in Fig. 2 (b) and (c) to identify the source of the possible degradation.

As shown in Fig. 2 (a), both the NDD and J_0 values for unfired samples show a decreasing trend at both dark annealing temperatures. Specifically, the NDD and J_0 of unfired samples decreased to -1.1×10^4 s^{-1} and 75.4 fA/cm^2 after 30 s of annealing at 380 °C. On the contrary, the NDD and J_0 of unirradiated fired samples show a different pattern than their unfired counterparts. The NDD and J_0 were relatively stable (0 ± 500 s^{-1} and 9.2 fA/cm^2) for a DA at 300 ° C, while we can see a gradual increase for a DA at 380 ° C. Although the highest NDD of unirradiated fired samples was only 2.45×10^3 s^{-1}, it still represents a 28.45 % loss of τ_{eff} compared to its original value. Thus, we can conclude that the unfired samples slightly improved during the dark annealing, benefiting from surface passivation, while the fired samples were relatively more stable during annealing.

To gain detailed insight into the effect of annealing on lifetime, three IDLS curves are plotted for both unfired and fired cases (380 ° C DA), as shown in Fig. 2(b) and (c). In Fig. 2 (b), it is notable that the τ_{eff} of the unfired samples at lower injection levels is considerably higher than at higher injection levels. However, the DA process significantly altered the shape of the IDLS curve. The τ_{eff} at MCD $> 10^{15}$ cm^{-3} increased from ~40 μ s to ~90 μ s after 120 s of annealing, while it was reduced from 65 μ s to 36 μ s at 4.3×10^{13}/cm^3 minority carrier density level. With further annealing process to 106,740 s, the τ_{eff} at low injection levels (MCD $< 10^{14}$ cm^{-3}) also became higher than the BoL values. Given the J_0 decrease observed in Fig. 2 (a), the improvement in lifetime of the unfired samples after annealing can likely be attributed to an improved surface passivation. Apart from the high injection region, the observed lifetime degradation at low injection levels may be related to the dissociation of FeGa complexes during high-temperature annealing [28, 29].

When looking into the IDLS curves for fired samples, as shown in Fig. 2 (c), the lifetime at higher injection levels slightly decreases at MCD $= 10^{16}$/cm^3 from 109 μ s to 101 μ s after 120 s, then to 74 μ s after 106,740 s of 380 ° C dark annealing process. Meanwhile, the change at low injection level (MCD $= 10^{14}$/cm^3) is negligible (from 117 μ s to 115 μ s after the annealing). This suggests that we mainly see a slight change in surface passivation, potentially attributed to the handling of the samples.

Overall, both the fired and unfired samples were found to be quite stable, indicating that the changes observed after irradiation can mainly be attributed to the irradiation-induced defects.

3.2. Impact of thermal annealing on irradiated silicon solar cells

3.2.1. Lifetime recovery from irradiation-induced damage

The injection-dependent lifetime as a function of annealing time at 300 ° C and 380 ° C are shown in Fig. 3. For all the samples presented in Fig. 3, the irradiation process significantly degraded the τ_{eff}, particularly at lower injection. The injection dependent τ_{eff} ranged from ~0.3 μ s to ~2.5 μ s for unfired and ~0.3 μ s to ~1.9 μ s for fired precursors after irradiation, with lower lifetime observed in lower injection levels. This suggests that the 1 MeV irradiation damage significantly impacted the performance of our precursors, and the effect on the lower injection level lifetime is more significant than that of the higher injection region.

The lifetime recovery of unfired samples is presented in Fig. 3 (a) and (b) under different annealing temperatures (300 ° C and 380 ° C). For unfired samples with 300 ° C DA shown in Fig. 3 (a), the lifetime at MCD $= 10^{15}$/cm^3 performed a gradual recovery of up to 72.46 % of its irradiation loss after 784,440 s (~193.7 h) dark annealing process, and it was not yet stabilized at the end of this study. By applying a slightly higher temperature of 380 ° C as shown in Fig. 3 (b), the lifetime recovery in unfired samples was clearly accelerated with 10,440 s (2.9 h) to regenerate 73.73 % of the lifetime loss at MCD $= 10^{15}$/cm^3. Meanwhile, the lifetime recovery kept increasing trend and finally was

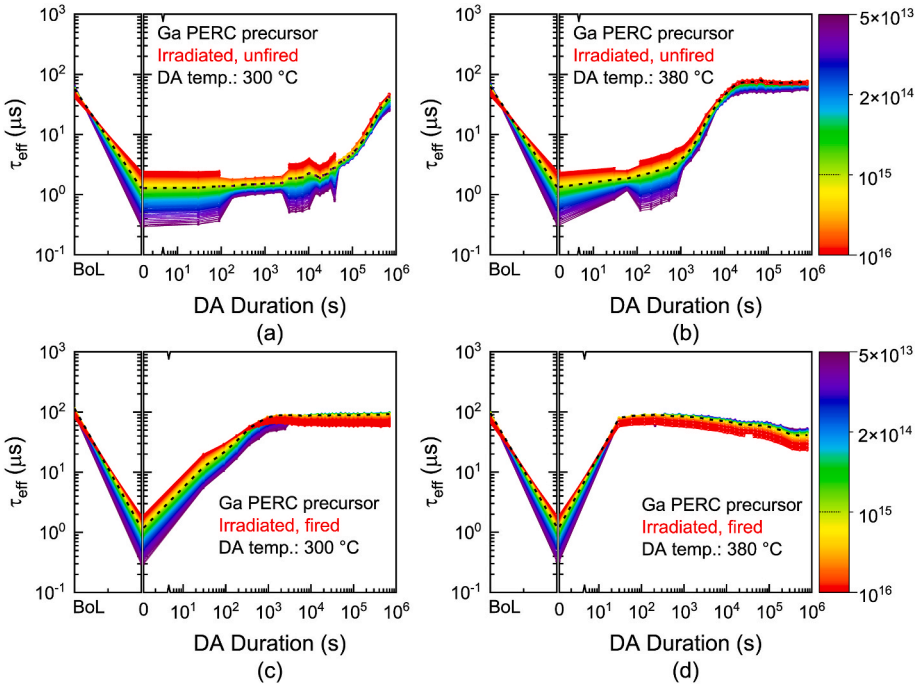

Fig. 3. IDLS measurements as a function of DA time for **unfired samples** with (a) 300 ° C, (b) 380 ° C DA and for **fired samples** with (c) 300 ° C, (d) 380 ° C DA; The injection level (MCD) ranges from 5×10^{13} to 10^{16}, the τ_{eff} at 10^{15} cm^{-3} is indicated as black dashed line as a reference. The lifetime at different injection levels is color-coded by a rainbow spectrum, with near-red indicating higher injection levels (up to 10^{16}/cm^3) and near-blue representing lower injection levels (down to 5×10^{13}/cm^3). The BoL IDLS measurement is shown in the figure as well. (For interpretation of the references to color in this figure legend, the reader is referred to the Web version of this article.)

stabilized after approximately 25,740 s (7.15 h) of 380 ° C annealing. It is worth noting that the τ_{eff} at higher injection levels was always higher than τ_{eff} at lower injection levels in the unfired samples during the annealing. The recovered lifetime of unfired samples became even higher than its original BoL values at higher injection levels ($\Delta n > \sim 3 \times 10^{14}/cm^3$), whereas the lifetime was lower than the BoL after the annealing for lower MCD values. As shown in Fig. 3 (b), the τ_{eff} at low injection level has not fully recovered after 784,440 s (221.07 h) of annealing. The $\tau_{eff,5e13}$ increased to 55 μ s at the end, corresponding to 83.97 % of BoL value.

Turning our attention to Fig. 3 (c) and (d), a significantly faster and better recovery was demonstrated in fired samples compared to the unfired peers. For the 300 ° C scenario in Fig. 3 (c), the fired samples only required 1560 s (~0.43 h) to recover an equivalent amount of the non-fired samples after 10,440 s, and τ_{eff} finally recovered to 92 μ s at $10^{15}/cm^3$ MCD. Furthermore, in Fig. 3 (d), the τ_{eff} regenerated to 79 μ s with only 30 s of annealing at 380 ° C, which is 83.14 % of its BoL value at a MCD value of $10^{15}/cm^3$ and finally achieved its highest τ_{eff} of 90 μ s after 210 s of annealing. A degradation of τ_{eff} was observed after reaching its maximum. The highest τ_{eff} at a MCD of $10^{16}/cm^3$ recovered 95.61 % of the irradiation losses, however, unlike the unfired samples, they did not exceed the BoL value. But interestingly, 92.8 % of τ_{eff} was regenerated at a low MCD of $\Delta n = 5 \times 10^{13}/cm^3$, which is significantly higher than the unfired case. As mentioned in Fig. 2, the degradation of the lifetime with the extended annealing period was attributed to the stability of the surface passivation.

Therefore, it is demonstrated that both fired and unfired samples can be recovered by dark annealing, particularly with higher annealing temperatures. In the unfired samples, the τ_{eff} at high injection levels can be fully recovered or even exceed the BoL value after the annealing process, similar as what was observed for the control samples shown in Fig. 2. However, τ_{eff} at low injection only can be partially recovered (83.97 % of BoL value at $5 \times 10^{13}/cm^3$) even with over 220 h of dark annealing at 380 ° C, whereas for fired samples, 92.8 % of τ_{eff} was recovered at a low MCD of $5 \times 10^{13}/cm^3$ after 540s annealing at 380 °C. Despite the slight decrease in surface passivation, the fired samples are more advantageous in terms of both recovery speed and quality compared to the unfired counterparts, particularly at low injection levels. This suggests that firing prior to the irradiation is an important process to accelerate the performance recovery in space silicon solar cells.

To access the degree of recovery of irradiation-induced defects, the NDD of irradiated Ga-PERC precursors are shown in Fig. 4 (a) at various stages: before irradiation (BoL), as-irradiated and annealing recovery, at an MCD = 10^{15} cm^{-3}. The IDLS curve of the BoL, as-irradiated, and recovered samples is also plotted in Fig. 4 (b) and (c) for both unfired and fired samples at 380 ° C, respectively.

As indicated in Fig. 4 (a), the NDD value increased remarkably to ~8 × 10^5 s^{-1} and ~7 × 10^5 s^{-1} after the electron irradiation for fired and unfired samples, respectively. During annealing, a gradual reduction in NDD for unfired samples was observed following the irradiation. Compared to the reference dashed line at NDD = 0, the NDD value even became negative, which is consistent with the results shown in Fig. 3 and can be related to an improved surface passivation. The recovery at 300 °C was approximately one order of magnitude slower. In contrast, as shown by the red lines in Fig. 4 (a), the fired irradiated Ga-PERC samples recovered quickly at both 300 ° C and 380 ° C, respectively, in a matter of 210 s and 1560 s. At 300 ° C, the NDD at $\Delta n = 10^{15}$ cm^{-3} decreased and stabilized from ~8 × 10^5 s^{-1} to 2.56 × 10^3 s^{-1} within 1560 s. The NDD of fired precursors took only 120 s to decrease to 1 × 10^3 s^{-1} at 380 ° C, whereas unfired samples required over 15,000 s at the same temperature. However, a continuous degradation was found in fired samples, with NDD ultimately rising to 1.4 × 10^4 s^{-1} after 784,440 s of 380 ° C annealing. Based on the results in Fig. 4(b) and (c), it becomes apparent that fired and unfired samples share similarities in their

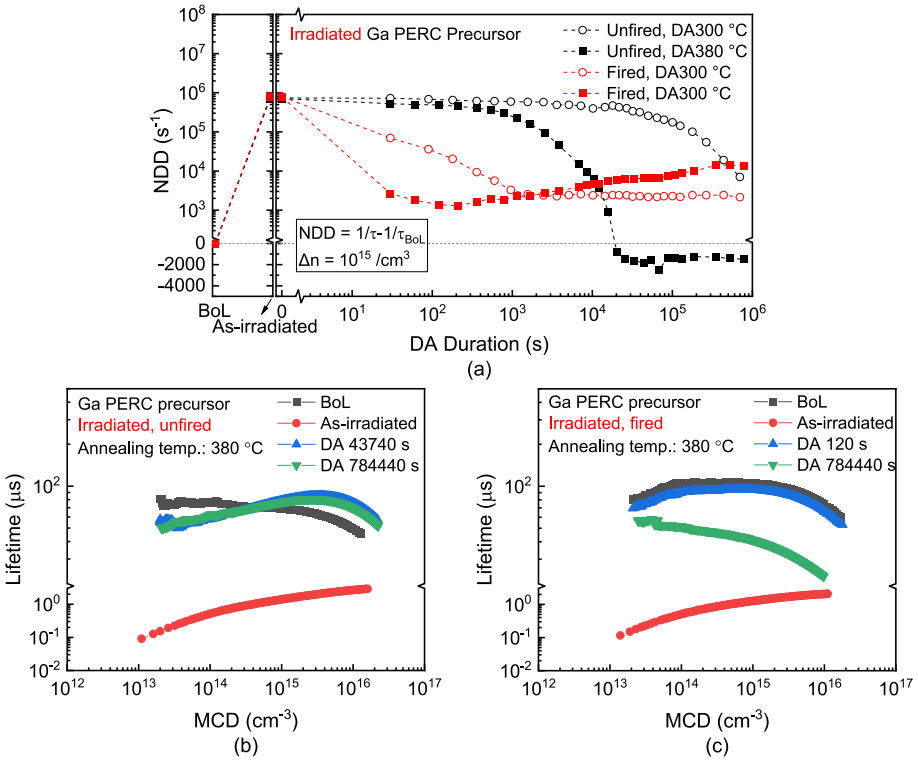

Fig. 4. (a) NDD results of irradiated unfired (black) and fired (red) PERC as a function of dark annealing time at $10^{15}/cm^3$, (b) injection-dependent effective lifetime of irradiated **unfired** PERC before irradiation (BoL, black), as-irradiated (red), then with 43740 s (blue) and 784440 s (green) of 380 ° C dark annealing, (c) injection dependent effective lifetime of irradiated **fired** PERC before irradiation (BoL, black), as-irradiated (red), then with 120 s (blue) and 784440 s (green) of 380 ° C dark annealing. (For interpretation of the references to color in this figure legend, the reader is referred to the Web version of this article.)

response to irradiation, while notable differences arise in the recovery process following irradiation. Despite the fact that only one set of samples was fired prior to irradiation, both sample types had a similar lifetime after irradiation, which was mainly determined by the irradiation-induced bulk defects. The relatively low temperature and short duration of the irradiation process were insufficient to result in a significant recovery of the irradiation-induced bulk defects. The introduced defects may include di-vacancies and other related complexes based on [19]. In terms of differences, the fired precursors demonstrated superior recovery speed and recovery ability compared to the unfired samples. This indicates a different irradiation recovery mechanism at play in the fired samples during the annealing process.

The injection-dependent lifetime curves are shown in Fig. 4 (b) and (c). The irradiation process degraded the BoL lifetime performance (black curves) of both fired and unfired samples to a similar level (red curves, ~1 μ s). However, the stabilized lifetime after annealing in unfired precursors showed a different injection dependency compared with its BoL results even after 784,440 s of dark annealing process. Compared to the BoL values, the annealed effective lifetimes became significantly higher at MCD >4 × 10^{14}/cm^3 while smaller at the lower injection levels. To be more specific, the BoL lifetime increased from 49 μ s to 71 μ s at 10^{16} cm^3 injection level, while decreasing from 76 μ s to 64 μ s at an injection level of 10^{14}/cm^3 at the end of this study. By comparison, the IDLS curve (blue) of recovered fired samples in Fig. 4 (c) was almost completely recovered to the BoL value (black) after 120 s dark annealing. However, a significant lifetime degradation (green) at high injection levels was observed with extended annealing. These results in Fig. 4(b) and (c) highlight the distinct responses of unfired and fired samples to the annealing recovery at both high and low injection levels. Similar to the control samples at high injection levels (see in Fig. 2), it is assumed that the annealing process can improve the surface passivation of unfired samples. At the same time, it was degraded for the fired case, in which the surface passivation instability is not directly correlated with the irradiation damage recovery. Apart from the surface passivation change, the bulk damage should also be effectively recovered after annealing. Given the recovery of τ_{eff} is attributed to both J_0 and τ_{SRH}, it is essential to isolate the recovery of irradiated bulk damage and surface passivation.

To quantitatively evaluate the irradiation damage and its recovery in bulk and surface, the injection-dependent recombination lifetime, τ_{SRH} and recombination current density J_0 were both extracted by fitting the measured data using Eq. (1). For simplicity, the τ_{s,J_0} was plotted to represent the front and rear J_0 value, that is calculated based on Eq. (1) as shown in Fig. 5. Apart from the BoL curve, the fitting was only carried out for recovered samples as the IDLS values for the irradiated samples were too low to quantify surface recombination.

Our study involved samples sourced from the same batch of an industrial silicon solar cell pilot line, leading us to consider τ_{rad} and τ_{Aug} as constant among these samples. In Fig. 5(a) and (b), we present the fitted results for the unfired sample at BoL (unirradiated) and recovered (after 784,440 s of 380 ° C annealing) state. The SRH defect assumed in the simulation is a deep-level defect, consistent with typical recombination centers affecting carrier lifetime. The final fitted effective lifetime $\tau_{eff,fit}$ in black dashed line showed good agreement with the raw data (black solid circles).

In Fig. 5 (a), the fitted τ_{SRH} were 478 μ s at an injection level of 10^{15}/cm^3 before irradiation with J_0 value equal to 212.27 fA/cm^2. With increased minority carrier injection density, the τ_{SRH} displayed an upward trend, ranging from 460 μ s at an MCD from 5 × 10^{13}/cm^3 to 581 μ s at 10^{16}/cm^3. Following the 784,440 s (217.9 h) of 380 ° C annealing process, both τ_{SRH} and J_0 significantly changed. Without changing the overall trend, the τ_{SRH} became more injection dependent where shifted with a higher value at high injection levels (1379 μ s at 10^{16}/cm^3) while became lower with lower carrier injections (130 μ s at 5 × 10^{13}/cm^3). Correspondingly, the τ_{SRH} was 301 μ s which was only 62.8 % of the BoL results at 10^{15}/cm^3 MCD, whereas the J_0 was nearly halved to 103.21 fA/cm^2. Thus, the effective lifetime curve shift in unfired samples after the annealing process was attributed to the reduced surface recombination losses and incomplete bulk damage recovery at low injection levels.

On the other hand, for fired samples, the difference in the fitted τ_{SRH} and J_0 between BoL and recovered values appeared insignificant, as shown in Fig. 5(c) and (d). Following the annealing, the J_0 value only showed a minimal increase from 148.36 fA/cm^2 to 169.10 fA/cm^2. And the τ_{SRH} was fully recovered at either low or high carrier injections. For instance, the τ_{SRH} of fired sample was restored to 7080 μ s, compared to its BOL value of 6784 μ s, at an MCD of 10^{15}/cm^3. These results show that the surface passivation in the fired precursors may have slightly degraded after the annealing. Still, the bulk damage was completely recovered, and the bulk electronic quality may even further improve.

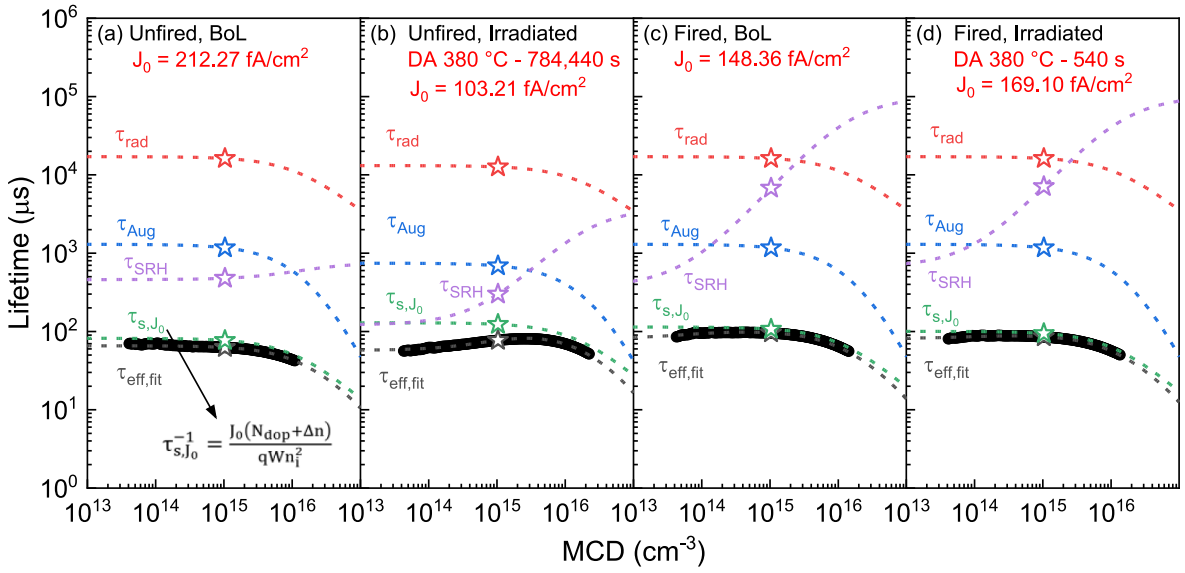

Fig. 5. Effective lifetime curve fitted using Eq. (1) for (a) unfired unirradiated sample (BoL), (b) unfired, irradiated sample after 784,440 s of 380 ° C annealing, (c) fired unirradiated sample (BoL) and (d) fired, irradiated sample after 540 s of 380 ° C annealing. The fitted results are plotted as dashed lines, with a highlighted lifetime (hollowed stars) at the MCD of 10^{15}/cm^3. The measured IDLS data is presented as solid black circles and the SRH defect assumed in the simulation is a deep-level defect, consistent with typical recombination centers affecting carrier lifetime.

Thus, it is obvious that the fired precursors not only show a faster recovery speed (see Fig. 4), but also better recovery quality (see Fig. 5) compared to the unfired samples. For a complete recovery of bulk damage in fired samples, it only requires around 540 s, which is about 71.5 times faster compared to reaching a stable recovery of τ_{eff} for the unfired samples. In addition, we find that the irradiation damage in unfired samples is incomplete (~46.4 %), even with 784,440 s (217.9 h) of annealing at the same condition.

As the firing process was the sole distinction between the unfired and fired samples, the bulk hydrogens from the firing process are a plausible explanation for the faster and complete recovery in fired samples. For the unfired samples, the recovery of irradiation-induced defects was primarily related to the reverse of irradiation damage, where the silicon self-interstitials interact with the irradiation-induced defects like vacancies. However, this recovery is insufficient to fully restore the bulk defects [30]. Whereas for the fired precursors, a substantial amount of hydrogen was injected from SiN_X:H [31–34], which can passivate defects in the c-Si bulk. These findings suggest that the hydrogenation process is critical to enhance the recovery ability of silicon space solar cells in terms of both speed and ability to achieve complete recovery.

3.2.2. Thermal donor during the annealing activity

Apart from lifetime recovery, the bulk conductivity of the silicon sample was also observed to have an increasing trend during the annealing, as shown in Fig. 6. As the irradiation-induced defects are commonly positively charged, particularly in p-type wafers [35], the reason for resistivity change will be explored in the following.

With the irradiation process, the resistivity did not show a significant change for the "BoL/As-irradiated" sample, with a value of 0.69 Ω cm for the irradiated unfired sample and 0.78 Ω cm for the irradiated fired sample, respectively. However, measured resistivity presents an increasing trend during the annealing process, particularly for the fired samples. In addition, the initial resistivity and changes after 352,440 s annealing were ~0.78 Ω cm and ~0.18 Ω cm for fired samples, which were significantly larger than the unfired samples with ~0.72 Ω cm and ~0.07 Ω cm. These changes correspond to a decrease in active Ga dopant concentration of ~2×10^{15}/cm^3 and ~4×10^{15}/cm^3 for both unfired and fired samples, respectively. However, since the resistivity did not change due to the irradiation process and the change was also detected for the control samples, this variation is not directly related to the irradiation damage and subsequent damage recovery. More likely,

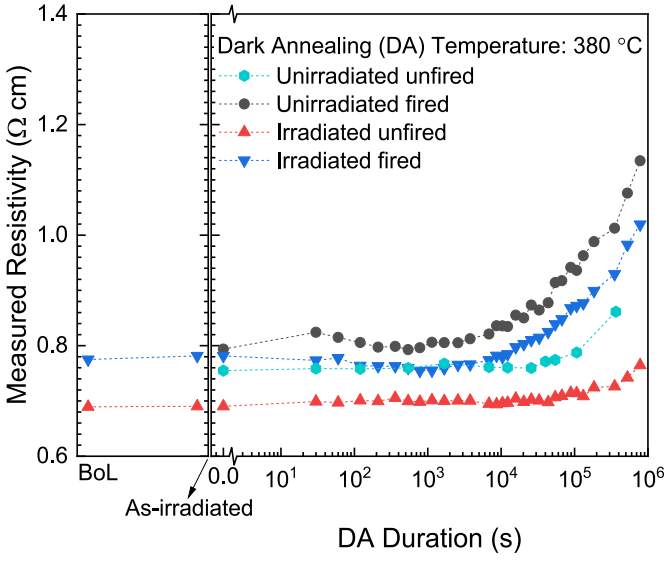

Fig. 6. Measured resistivity of Ga PERC samples during the dark annealing process. The resistivity was determined from conductance measurements in the dark.

these variations were attributed to the oxygen thermal donors that formed during the 380 ° C annealing process [36], or associated with a decreased number of active dopants due to the diffused hydrogen [37]. However, to mitigate the large discrepancy in Ga dopant concentration between the fired and unfired samples, a hydrogen concentration of 4×10^{15}/cm^3 would have been required. Such a high hydrogen concentration is unlikely to be diffused into the silicon bulk region during firing. Moreover, this variation does not seem to be driven by hydrogen, as similar resistivity changes were also observed in the unfired samples. Therefore, the formation of GaH_2 complex does not appear to explain the observed resistivity difference. Instead, the thermal donor theory is a possible explanation, and the firing process can introduce additional thermal donor precursors/species, which accelerated thermal donor generation in the fired samples during the 380 ° C annealing.

Moreover, although resistivity shows a constant increase, the trend of resistivity change exhibits different patterns that vary over a lifetime during the annealing process. Meanwhile, the resistivity of all our samples did not show significant change due to irradiation. This suggests that the thermal donor we observed may not directly impact the monitoring of the bulk lifetime change from irradiation loss and following recovery.

3.3. Monitoring of bulk defects variation by DLTS method

Various DLTS samples were prepared based on the extent of lifetime recovery shown in Fig. 4. In each group, three small tokens were cleaved from the same sample at different time stamps of 380 ° C annealing process. A summary of DLTS signals and corresponding defect parameters are shown in Fig. 7.

The DLTS results for unfired samples are shown in Fig. 7 (a) for unirradiated samples and (b) for irradiated samples. Two signals were obtained for the unirradiated unfired samples, including H135 and H165, as shown in Fig. 7 (a), with a small apparent capture cross-section value of 4.6×10^{-19} cm^2 and 9.3×10^{-18} cm^2, respectively. The defect density of H165 decreased from 3.65×10^{13}/cm^3 to 2.18×10^{13}/cm^3 after 30,000 s of annealing and finally under the detection limit in the following annealing. While the H135 defects were only observed after 30,000 s of annealing. Based on the small apparent capture cross-section of H135 and H165, they are likely to be electrically active but not recombination active. H135 defects may be a transitional form of other traps or introduced during the annealing process.

However, in the irradiated unfired sample, as shown in Fig. 7 (b), two new defects, H150 and H230, were identified in the DLTS measurements. H150 was observed before annealing with a trap energy $E_V + E_\infty = 0.23$ eV and apparent capture cross-section $\sigma_a = 1.5 \times 10^{-16}$ cm^2. And it was only found in the as-irradiated sample with a 4.73×10^{13}/cm^{-3} of trap density. Meanwhile, H230 was detected in the irradiated unfired sample when the lifetime was fully recovered and was not observed in the sample at the over-annealed stage. However, in Fig. 7 (b), due to the overlap with H150 defect peak, the same defect peak as H165 in Fig. 7 (a) appeared to be shifted 10 K higher and shows as H175. Both of them shared similar defects property as shown in the table. By comparing with previous literature, the trap parameters of H150 match those of a donor state of the divacancy trap observed in silicon samples after irradiation [10,15]. These defects were introduced by irradiation and subsequently removed during the annealing process. H230 is unlikely to be a recombination active defect as the activation energy and the apparent capture cross-section of the H230 trap are both small, too.

In the fired control sample, it was observed that the DLTS detected levels H145, H230, and H240 have relatively small activation energy and apparent capture cross-section, as shown in Fig. 7 (c), indicating that they are unlikely to cause lifetime reduction, and this matches with the lifetime results in Fig. 2 (c). Moreover, H240 is likely to be metastable in the 380 ° C annealing process as its density decreased and then increased as a function of the annealing time.

H195 and H235 were observed in the as-irradiated fired samples, and

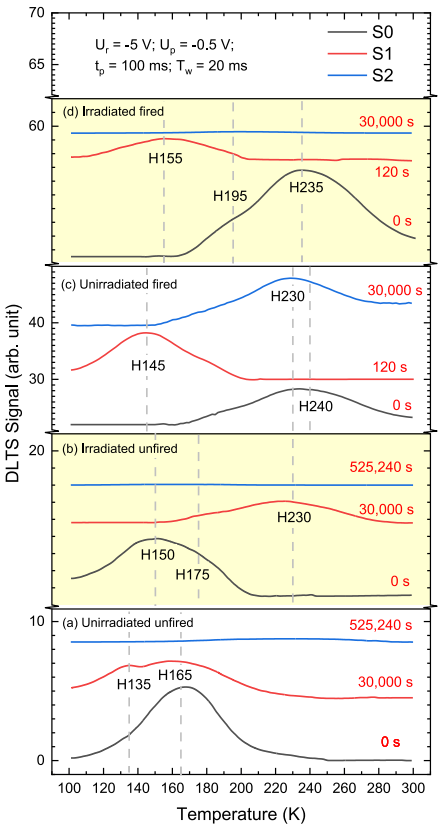

Stage and corresponding DA duration (s)			
Stage	S0	S1	S2
Fired	0	120	30000
Unfired	0	30000	525240

Irradiated fired			
Traps	H155(C_i)	H195 (V-V^+)	H235 (C_i-C_s)
E_V+E_∞ (eV)	0.27	0.21	0.33
σ_a (cm^2)	6.6×10^{-18}	2.9×10^{-16}	7.7×10^{-17}
S0 N_t (cm^{-3})	-	1.32×10^{13}	5.58×10^{13}
S1 N_t (cm^{-3})	7.42×10^{12}	-	-
S2 N_t (cm^{-3})	-	-	-

Unirradiated fired			
Traps	H145	H230	H240
E_V+E_∞ (eV)	0.18	0.14	0.19
σ_a (cm^2)	7.1×10^{-18}	8.4×10^{-21}	2.0×10^{-19}
S0 N_t (cm^{-3})	-	-	2.37×10^{13}
S1 N_t (cm^{-3})	8.23×10^{12}	-	-
S2 N_t (cm^{-3})	-	7.36×10^{13}	4.66×10^{13}

Irradiated unfired			
Traps	H150 (V-V^+)	H175	H230
E_V+E_∞ (eV)	0.23	0.18	0.02
σ_a (cm^2)	1.5×10^{-16}	9.0×10^{-18}	1.5×10^{-23}
S0 N_t (cm^{-3})	4.73×10^{13}	6.82×10^{12}	-
S1 N_t (cm^{-3})	-	2.67×10^{12}	1.11×10^{13}
S2 N_t (cm^{-3})	-	-	-

Unirradiated unfired		
Traps	H135	H165
E_V+E_∞ (eV)	0.2	0.18
σ_a (cm^2)	4.6×10^{-19}	9.3×10^{-18}
S0 N_t (cm^{-3})	-	3.65×10^{13}
S1 N_t (cm^{-3})	1.96×10^{13}	2.18×10^{13}
S2 N_t (cm^{-3})	-	-

Fig. 7. DLTS spectra (left) for (a) unirradiated unfired samples; (b) irradiated unfired samples; (c) unirradiated fired samples; (d) irradiated fired samples; **corresponding defect parameters/density changes (right)** at different annealing stages: as-irradiated (S0; in black), after 380 ° C DA till lowest NDD achieved (S1: with 120 s for fired and 30,000 s for unfired samples, colored in red) and after 380 ° C DA for an extended time (S2: , with 30,000 s for fired samples and 525,240 s for unfired, colored in blue). * – : under detection limit. (For interpretation of the references to color in this figure legend, the reader is referred to the Web version of this article.)

they were eventually annealed out after 120 s of annealing when the H155 defect was found. H195 was observed before annealing, and it was found to have defect parameters that were close to H150, as detected in the irradiated unfired sample [see Fig. 7 (c)]. Therefore, H195 is also considered to be the same donor state as V-V defect [10,15]. The shift of the peak on the temperature axis is due to its overlapping with H235 in the spectrum, which also lead to the H240 in control samples shifted to H235 in the irradiated case. H235 and H155 aligned with the electrical properties of C_i-C_s and C_i, respectively [38].

Eventually, all these levels were annealed out, as listed in Fig. 7, after an extended annealing time (525,240 s for unfired and 30,000 s for fired) at 380 ° C. Although the standard DLTS measures majority-carrier traps rather than detecting the minority-carrier trap, our results revealed signals associated with vacancy-related defects, particularly divacancies (V-V^+), which are well-known in irradiated silicon solar cells. We acknowledge multiple defect species such as V_2 (V-V^+), V_3 and V-O complexes [37] are also expected in the irradiated silicon, however, their contribution to the carrier recombination in our precursors may not significant. Thus, we hypothesize that the divacancies are the dominant defects responsible for the irradiation induced losses in our PERC precursors. Meanwhile, V-V^+, C_i-C_s and C_i levels were also found in the irradiated fired samples, which are all donor defects [38]. However, these defects have significantly low density compared to the dopant density changes during annealing. This suggests that the changes in resistivity observed in Fig. 6 are likely influenced by other factors (thermal donors), rather than the irradiation induced defects.

4. Conclusion

In this study, we have compared the electron irradiation losses and subsequent recovery of unfired and fired Ga-PERC precursors. Both samples showed a similar decrease in minority carrier lifetime after electron irradiation, but they showed significant differences in the following recovery dynamics. The fired samples showed complete recovery after only 540 s at 380 ° C, which is 71.5 times faster than non-fired samples that saturated at 46.4 % of the initial lifetime. Considering that the firing process was the only difference between the two samples, we believe that the bulk hydrogen in fired samples significantly improves the self-healing efficiency of the PERC precursors.

From DLTS analysis, it was further confirmed that the main bulk damage could be completely recovered for both fired and unfired samples, including two major irradiation-induced defects in the bulk, V-V^+ and C_i-C_s. However, it was also noted that a prolonged annealing process in fired samples may cause degradation of surface passivation [37] and change in resistivity, which are both not related to the irradiation damage and recovery.

In conclusion, our work demonstrated that bulk hydrogenation is extremely advantageous for Ga-doped PERC solar cells as it allows for significantly faster (up to two orders of magnitude) recovery of irradiation-induced damage. We propose that Ga-PERC solar cells with extensive bulk hydrogenation are optimal for short-term LEO space missions. They can be produced at a cost comparable to terrestrial silicon solar cells and can self-repair electron radiation damage during operation.

CRediT authorship contribution statement

Guo Li: Writing – review & editing, Writing – original draft, Visualization, Validation, Resources, Methodology, Investigation, Formal analysis, Data curation, Conceptualization. **Zhuangyi Zhou:** Writing –

review & editing, Writing – original draft, Formal analysis, Data curation. **Chukwuka Madumelu:** Writing – review & editing. **Peter Toth:** Writing – review & editing. **Lennart van den Hengel:** Resources. **Ferdinand Grozema:** Resources. **Gavin Conibeer:** Writing – review & editing, Supervision, Project administration, Funding acquisition. **Bram Hoex:** Writing – review & editing, Visualization, Supervision, Project administration, Funding acquisition, Conceptualization.

Declaration of competing interest

The authors declare the following financial interests/personal relationships which may be considered as potential competing interests:

Guo Li reports financial support was provided by China Scholarship Council. If there are other authors, they declare that they have no known competing financial interests or personal relationships that could have appeared to influence the work reported in this paper.

Acknowledgements

Guo Li would like to thank the financial support provided by the China Scholarship Council (project ID 202108200014). The authors acknowledge support by the Australian Government through the Australian Research Council's Linkage and Discovery schemes (projects DP220101532, DP170102677, LP210100426 & LP210200883). The authors are grateful to Brendan Wright at UNSW for assisting in the lifetime fitting.

Data availability

Data will be made available on request.

References

[1] R.L. Easton, M.J. Votaw, Vanguard I IGY Satellite (1958 Beta), Rev. Sci. Instrum. 30 (2) (1959) 70–75, https://doi.org/10.1063/1.1716492.
[2] D.J. Flood, Space photovoltaics – History, progress and promise, Mod. Phys. Lett. B 15 (17n19) (2001) 561–570, https://doi.org/10.1142/s0217984901002038.
[3] B.E. Anspaugh, Proton and electron damage coefficients for GaAs/Ge solar cells, in: Presented at the the Conference Record of the Twenty-Second IEEE Photovoltaic Specialists Conference - 1991, vol. 2, 1991, pp. 1593–1598, https://doi.org/10.1109/PVSC.1991.169472.
[4] H. Afshari, et al., Radiation tolerance of GaAs1-xSbx solar cells, Sol. Energy Mater. Sol. Cell. 233 (Dec. 2021) 111352, https://doi.org/10.1016/j.solmat.2021.111352.
[5] J. Schoen, et al., Improvements in ultra-light and flexible epitaxial lift-off GaInP/GaAs/GaInAs solar cells for space applications, Prog. Photovoltaics 30 (8) (Aug. 2022) 1003–1011, https://doi.org/10.1002/pip.3542.
[6] A. Wang, High Efficiency PERC and PERL Silicon Solar Cells, PhD Thesis, 1992, https://doi.org/10.26190/unsworks/4395.
[7] M. Yamaguchi, S.J. Taylor, S. Matsuda, O. Kawasaki, Mechanism for the anomalous degradation of Si solar cells induced by high fluence 1 MeV electron irradiation, Appl. Phys. Lett. 68 (22) (1996) 3141–3143, https://doi.org/10.1063/1.115804.
[8] NREL's Best Research-Cell Efficiency Chart," vol. 2023, no. 06 June, [Online]. Available: https://www.nrel.gov/pv/cell-efficiency.html.
[9] K.A. Horowitz, T.W. Remo, B. Smith, A.J. Ptak, A Techno-Economic Analysis and Cost Reduction Roadmap for III-V Solar Cells, Office of Scientific and Technical Information (OSTI), 2018, https://doi.org/10.2172/1484349.
[10] M. Yamaguchi, et al., Deep level analysis of radiation-induced defects in Si crystals and solar cells, J. Appl. Phys. 86 (1) (1999) 217–223, https://doi.org/10.1063/1.370698.
[11] A. Khan, et al., Strategies for improving radiation tolerance of Si space solar cells, Sol. Energy Mater. Sol. Cell. 75 (1) (2003) 271–276, https://doi.org/10.1016/S0927-0248(02)00169-1.
[12] D.-H. Neuhaus, A. Münzer, Industrial silicon wafer solar cells, Adv. Optoelectron. 2007 (2007).
[13] J. Lindroos, H. Savin, Review of light-induced degradation in crystalline silicon solar cells, Sol. Energy Mater. Sol. Cell. 147 (2016) 115–126, https://doi.org/10.1016/j.solmat.2015.11.047.
[14] F. Hartmann, Evolution of Silicon Sensor Technology in Particle Physics, vol. 231, Springer Tracts in Modern Physics, 2009, https://doi.org/10.1007/b106762.
[15] G.D. Watkins, J.W. Corbett, Defects in irradiated silicon: electron paramagnetic resonance and electron-nuclear double resonance of the Si-E center, Phys. Rev. 134 (5A) (Jun. 1964) A1359–A1377, https://doi.org/10.1103/PhysRev.134.A1359.
[16] G.D. Watkins, Intrinsic defects in silicon, Mater. Sci. Semicond. Process. 3 (4) (2000) 227–235, https://doi.org/10.1016/S1369-8001(00)00037-8.
[17] P.A. Iles, Evolution of space solar cells, Sol. Energy Mater. Sol. Cell. 68 (1) (2001) 1–13, https://doi.org/10.1016/S0927-0248(00)00341-X.
[18] S. Bailey, R. Raffaelle, Space solar cells and Arrays, in: Handbook of Photovoltaic Science and Engineering, 2003, pp. 413–448, https://doi.org/10.1002/0470014008.ch10.
[19] A. Khan, M. Yamaguchi, S.J. Taylor, T. Hisamatsu, S. Matsuda, Effects of annealing on type converted Si and space solar cells irradiated with Heavy fluence 1 MeV electrons, Jpn. J. Appl. Phys. 38 (5R) (1999), https://doi.org/10.1143/jjap.38.2679, pp. 2679–2679.
[20] C.E. Barnes, G.A. Samara, Forward bias induced annealing of the E center in silicon, Appl. Phys. Lett. 48 (14) (1986) 934–936, https://doi.org/10.1063/1.96663.
[21] G.D. Watkins, J.W. Corbett, Production of divacancies and vacancies by electron irradiation of silicon, Phys. Rev. 138 (2A) (1965) A543–A555, https://doi.org/10.1103/physrev.138.a543.
[22] W.E. Horne, Predicting annealing of Lithium-doped solar cells during long duration space missions, IEEE Trans. Nucl. Sci. 23 (6) (Dec. 1976) 1803–1807, https://doi.org/10.1109/TNS.1976.4328581.
[23] N. Nagai, H. Ishida, T. Hisamatsu, T. Aburaya, S. Matsuda, FT-IR study of electron- or proton-irradiated Si crystals for solar cells, J. Cryst. Growth 210 (1) (2000) 74–79, https://doi.org/10.1016/S0022-0248(99)00650-8.
[24] J. Kuendig, A. Shah, Effect of proton irradiation and subsequent thermal annealing on the characteristics of thin-film silicon solar cells and microcrystalline silicon layers, IEEE (2002), https://doi.org/10.1109/pvsc.2002.1190763.
[25] M.U. Khan, et al., Degradation and regeneration of radiation-induced defects in silicon: a study of vacancy-hydrogen interactions, Sol. Energy Mater. Sol. Cell. 200 (2019), https://doi.org/10.1016/j.solmat.2019.109990, pp. 109990–109990.
[26] J. Schmidt, R.A. Sinton, Defect characterization by temperature and injection-dependent lifetime spectroscopy, in: Presented at the 3rd World Conference onPhotovoltaic Energy Conversion, 2003. Proceedings of, 2003, vol. 1, 2003, pp. 947–950.
[27] S.W. Glunz, S. Rein, W. Warta, J. Knobloch, W. Wettling, Degradation of carrier lifetime in Cz silicon solar cells, Sol. Energy Mater. Sol. Cell. 65 (1) (Jan. 2001) 219–229, https://doi.org/10.1016/S0927-0248(00)00098-2.
[28] G. Zoth, W. Bergholz, A fast, preparation-free method to detect iron in silicon, J. Appl. Phys. 67 (11) (Jun. 1990) 6764–6771, https://doi.org/10.1063/1.345063.
[29] T.U. Nærland, et al., On the recombination centers of iron-gallium pairs in Ga-doped silicon, J. Appl. Phys. 122 (8) (Aug. 2017) 085703, https://doi.org/10.1063/1.5000358.
[30] B.J. Hallam, P.G. Hamer, A.M. Ciesla née Wenham, C.E. Chan, B. Vicari Stefani, S. Wenham, Development of advanced hydrogenation processes for silicon solar cells via an improved understanding of the behaviour of hydrogen in silicon, Prog. Photovoltaics Res. Appl. 28 (12) (2020) 1217–1238, https://doi.org/10.1002/pip.3240.
[31] J. Schmidt, et al., Advances in the surface passivation of silicon solar cells, Energy Proc. 15 (2012) 30–39, https://doi.org/10.1016/j.egypro.2012.02.004.
[32] A. Cuevas, et al., Carrier population control and surface passivation in solar cells, Sol. Energy Mater. Sol. Cell. 184 (2018) 38–47, https://doi.org/10.1016/j.solmat.2018.04.026.
[33] J. Schmidt, R. Peibst, R. Brendel, Surface passivation of crystalline silicon solar cells: present and future, Sol. Energy Mater. Sol. Cell. 187 (2018) 39–54, https://doi.org/10.1016/j.solmat.2018.06.047.
[34] A. Cuevas, T. Allen, J. Bullock, Y. Wan, D. Yan, X. Zhang, Skin care for healthy silicon solar cells, in: 2015 IEEE 42nd Photovoltaic Specialist Conference (PVSC), Jun. 2015, pp. 1–6, https://doi.org/10.1109/PVSC.2015.7356379.
[35] M. Yamaguchi, K.-H. Lee, K. Araki, N. Kojima, Y. Okuno, M. Imaizumi, Analysis for nonradiative recombination loss and radiation degradation of Si space solar cells, Prog. Photovoltaics Res. Appl. 29 (2020), https://doi.org/10.1002/pip.3346.
[36] W. Wijaranakula, Formation kinetics of oxygen thermal donors in silicon, Appl. Phys. Lett. 59 (13) (Sep. 1991) 1608–1610, https://doi.org/10.1063/1.106245.
[37] V.P. Markevich, A.R. Peaker, S.B. Lastovskii, V.E. Gusakov, I.F. Medvedeva, L. I. Murin, Formation of radiation-induced defects in Si crystals irradiated with electrons at elevated temperatures, Solid State Phenom. 156–158 (2010) 299–304. https://doi.org/10.4028/www.scientific.net/SSP.156-158.299.
[38] E. Borchi, M. Bruzzi, Z. Li, S. Pirollo, Thermally stimulated currents analysis of the shallow levels in irradiated silicon detectors, J. Phys. D Appl. Phys. 33 (3) (Feb. 2000) 299, https://doi.org/10.1088/0022-3727/33/3/318.